Controlling In-cylinder Composition on Turbocharged Variable-Valve-Timing Spark Ignition Engines

Thomas Leroy, Jonathan Chauvin and Nicolas Petit

Abstract— **We consider a spark-ignition engine equipped with VVT actuators. This paper is an extension of a previously studied control technique (considered under atmospheric conditions). We show that the same control strategy boosts the torque production using VVT actuators under turbocharging conditions. At the light of reported experimental results, we stress the performance of the proposed control law and prove its theoretical beneficial effects.**

I. Introduction and motivations

In this paper, we consider a Spark-Ignition (SI) engine equipped with a turbocharger and two Variable-Valve-Timing (VVT) devices. Such an engine setup is designed to maximize performance under steady-state conditions, at the expense of an increased complexity, and a dynamical behavior which is challenging from an automatic control standpoint. The engine setup is represented in Figure 1. The cylinders are fed with fresh air from the throttle which is located downstream a compressor. The compressor is powered by the turbine located downstream the exhaust manifold. Indirectly, the waste gate controls the compression rate. VVT actuators independently impact on the timing of the intake and exhaust phases. Finally, combustion of the injected fuel takes place in the cylinders.

On general SI engines, the engine torque output is directly determined by the in-cylinder trapped air mass at intake valve closing (assuming an air/fuel ratio controller is in service) (see [1]). On engines equipped with VVT actuators, the in-cylinder fresh air charge is impacted by the valves lifts. During a variable time called "overlap period", both valves are opened simultaneously. Under atmospheric conditions, the intake manifold pressure is lower than the exhaust manifold pressure. This permits to increase the in-cylinder burned gas fraction, which reduces pumping losses and yields fuel economy [1]. Under turbocharging conditions, the intake manifold pressure is higher than the exhaust manifold pressure. Then, the residual gases are flushed out of the cylinder by sending fresh air directly to the exhaust [2]. This internal gas recirculation affects the fresh air charge. Because no sensor can be placed inside the combustion chamber (due to the high cost of such an in-situ installation), remote sensors and model-based observers must be considered to estimate the fresh air charge. Obviously, VVT actuators positions have to be taken into account into such models (this can be done using a mean-value model of the aspirated air mass of such an engine such as given in [3]).

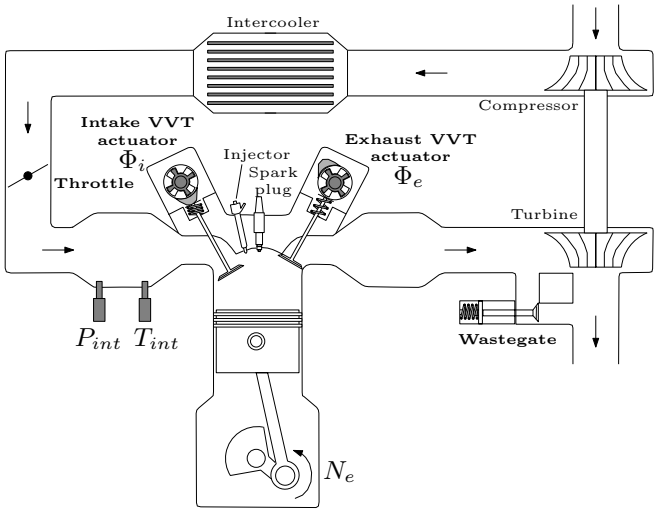

Fig. 1. Engine scheme. Intake manifold pressure and temperature, P_{int} and T_{int}, are measured by sensors. Φ_i and Φ_e are VVT actuators positions and N_e is the engine speed.

In-cylinder composition is directly linked to intake manifold pressure and VVT actuators positions. Because of the different time responses of these quantities, control of the in-cylinder composition can be affected [4], causing driveability problems and pollution peaks. In [5], we proposed a control strategy taking into account the differences in the dynamics of the system. In details, we proceeded as follows. Consider a typical turbocharged VVT SI engine, whose control system includes a low-level intake manifold pressure controller, and two low-level VVT controllers. Such controllers are exposed in [6], [7], [8], [9] for example. In closed-loop, the intake manifold subsystem and the VVT subsystems have varying performances (mainly speed of convergence) over the whole engine conditions range. Their responses can be considered as moderately fast to slow, and, at occasions, they can outperform each other. A primary control objective is the aspirated air mass (because it directly impacts torque production). A secondary control objective is the Internal Gas Recirculation (IGR) mass (extra control objective in an attempt to move forward in the direction of combustion control). The strategy we proposed in [5] aims at coordinating the three low-level control subsystems to improve the overall performance.

In [5], we focused on atmospheric conditions. In this

T. Leroy (corresponding author) is a PhD Candidate in Mathematics and Control, Centre Automatique et Systèmes, École des Mines de Paris, 60, bd St Michel, 75272 Paris, France.
Email: *thomas.leroy@ensmp.fr*

J. Chauvin is with the Department of Engine Control in Institut Français du Pétrole, 1 et 4 Avenue de Bois Préau, 92852 Rueil Malmaison, France

N. Petit is with the Centre Automatique et Systèmes, École des Mines de Paris, 60, bd St Michel, 75272 Paris, France

ISBN 978-963-311-369-1

working area, intake manifold pressure is controlled with the intake throttle and its dynamics satisfies a fast first order dynamics (see [10] for example). Meanwhile, hydraulic VVT actuators dynamics are slow compared to the one of the intake manifold pressure. We have shown that a better way to control the aspirated air mass is to control it with the intake manifold pressure (because VVT are saturated actuators). On the other hand, VVT actuators control the second objective which is the IGR mass. By using measurements of pressure and VVT actuators positions in the control strategy, we improve the overall performance. VVT actuators measurements are used in the pressure trajectory generation. This permits to improve the aspirated air mass transient behavior.

In this paper, we focus on turbocharging conditions. In this working area, intake manifold pressure can be seen as the slow variable of the system. Actually, the throttle is wide open and the turbo-lag limits time response of the intake pressure. Here, VVT actuators are seen as the fast control variables. Despite these differences in operating conditions, we show that the exact same control strategy as in [5] also permits to improve the aspirated air mass (and then torque) response during a fast torque tip-in. Further, we analyze the transient behavior from a theoretical point of view.

The paper is organized as follows. In Section II, we present a model of the in-cylinder composition. Section III exposes the control strategy. Experimentally, and theoretically, the proposed control strategy is compared against a "static" controller during a fast torque tip-in in Section IV. Finally, we conclude and give future directions.

II. Modeling

A. Model definition

Notations are given in Table I. Consider a turbocharged SI engine equipped with an intake throttle, a waste gate and two dual independent VVT actuators as depicted in Figure 1.

TABLE I
NOMENCLATURE

Symbol	Description	Unit	Variable
m_{asp}	Aspirated air mass	kg	y_1
m_{igr}	Internal gas recirculation mass	kg	y_2
N_e	Engine speed	rpm	
OF	Overlap factor	$m^2 \cdot \deg$	
P_{int}	Intake manifold pressure	Pa	x_1
Φ_i	Intake VVT actuator position	deg	x_2
Φ_e	Exhaust VVT actuator position	deg	x_3
R	Ideal gas constant	$J/(kg \cdot K)$	
T_{int}	Intake manifold temperature	K	
V_{ivc}	In-cylinder volume at ivc	m^3	
V_{evc}	In-cylinder volume at ivc	m^3	

An aspirated air and IGR masses model for such an engine has been presented in [3]. It simply involves variables which can be estimated from in-line commercial sensors (engine speed, intake manifold pressure and temperature, and VVT actuators positions). Let m_{asp} and m_{igr} be the aspirated air mass and the IGR mass, respectively. The model writes

$$\begin{cases} m_{igr} \triangleq \alpha_2 \dfrac{\mathrm{OF}(\Phi_i, \Phi_e)}{N_e} + \alpha_3 V_{evc}(\Phi_e) \\ m_{asp} \triangleq \alpha_1 \dfrac{P_{int} V_{ivc}(\Phi_i)}{R T_{int}} - m_{igr} \end{cases} \tag{1}$$

where α_1, α_2 and α_3 are known functions of P_{int} and N_e. V_{ivc} is the cylinder volume at intake valve closing (ivc). It is a function of intake valve timing, Φ_i. Similarly, V_{evc} is the cylinder volume at exhaust valve closing (evc). It is a function of exhaust valve timing, Φ_e. At last, the overlap factor (OF) is a function of both the intake and exhaust VVT, Φ_i and Φ_e.

IGR mass, m_{igr}, can become negative when the engine is operating under turbocharging conditions (see [3]). Under these conditions, m_{igr} does not model the in-cylinder burned gas mass but the fresh air that is sent directly to the exhaust (thanks to a positive pressure difference between intake and exhaust manifolds).

B. State space model

Let $\Omega_{\Phi_i} = \left[\Phi_i^{\min}; \Phi_i^{\max}\right]$ be the set of feasible intake VVT actuator positions. Respectively, let $\Omega_{\Phi_e} = \left[\Phi_e^{\min}; \Phi_e^{\max}\right]$ be the set of admissible exhaust VVT actuator positions. Let $\Omega_p = \left[P_{int}^{\min}; P_{int}^{\max}\right]$ be the set of considered intake manifold pressure. Let Ω_{air} be the set of feasible air mass, and, finally, Ω_{igr} be the set of feasible IGR mass.

We note $f : \Omega_p \times \Omega_{\Phi_i} \times \Omega_{\Phi_e} \longrightarrow \mathbb{R}$ and $g : \Omega_p \times \Omega_{\Phi_i} \times \Omega_{\Phi_e} \longrightarrow \mathbb{R}$ such that $m_{asp} \triangleq f(P_{int}, \Phi_i, \Phi_e)$ and $m_{igr} \triangleq g(P_{int}, \Phi_i, \Phi_e)$.

Let $x \triangleq [P_{int} \ \ \Phi_i \ \ \Phi_e]^T$ and $y \triangleq [m_{asp} \ \ m_{igr}]^T$ be the state and the output of the system respectively. To simplify the theoretical analysis, one can assume pressure and VVT subsystems as first order systems. Dynamics writes

$$\begin{cases} \dot{x}_1 = \psi(y_1)(-x_1 + x_1^{sp}) \\ \dot{x}_2 = \gamma_2(-x_2 + x_2^{sp}) \\ \dot{x}_3 = \gamma_3(-x_3 + x_3^{sp}) \\ y_1 = f(x_1, x_2, x_3) \\ y_2 = g(x_1, x_2, x_3) \end{cases} \tag{2}$$

where x_1^{sp}, x_2^{sp} and x_3^{sp} are the intake manifold pressure, the intake VVT position and the exhaust VVT position set points respectively. γ_2 and γ_3 are positive constants. The mapping $\psi : \Omega_{air} \to \mathbb{R}^+$ is a constant under atmospheric conditions and is an increasing function under turbocharging conditions.

C. Model properties

1) Inversibility properties: Due to the structure of α_1, α_2, α_3, OF, V_{ivc} and V_{evc} as functions of x_1, x_2, x_3, the three following partial inversibility assumptions hold (all the variables structures are given in [3]).

Assumption 1. *For all $(x_2, x_3, y_1) \in \Omega_{\Phi_i} \times \Omega_{\Phi_e} \times \Omega_{air}$, there exists a unique $x_1 \in \Omega_p$ such that $f(x_1, x_2, x_3) = y_1$.*

Assumption 2. *For all $(x_1, x_3, y_2) \in \Omega_p \times \Omega_{\Phi_e} \times \Omega_{igr}$, there exists a unique $x_2 \in \mathbb{R}$ such that $g(x_1, x_2, x_3) = y_2$.*

Assumption 3. *For all* $(x_1, x_2, y_2) \in \Omega_p \times \Omega_{\Phi_i} \times \Omega_{igr}$*, there exists a unique* $x_3 \in \mathbb{R}$ *such that* $g(x_1, x_2, x_3) = y_2$.

From the above assumptions, (partial) inverse functions of f and g can be defined. We note $f^{-1}_{x_2,x_3} : \Omega_{air} \rightarrow \Omega_p$, $g^{-1}_{x_1,x_3} : \Omega_{igr} \rightarrow \Omega_{\Phi_i}$ and $g^{-1}_{x_1,x_2} : \Omega_{igr} \rightarrow \Omega_{\Phi_e}$ which are implicitly defined by the following relations holding for all $(x_1, x_2, x_3) \in \Omega_p \times \Omega_{\Phi_i} \times \Omega_{\Phi_e}$

$$y_1 = f(x_1 = f^{-1}_{x_2,x_3}(y_1), x_2, x_3) \quad (3a)$$
$$y_2 = g(x_1, x_2 = g^{-1}_{x_1,x_3}(y_2), x_3) \quad (3b)$$
$$y_2 = g(x_1, x_2, x_3 = g^{-1}_{x_1,x_2}(y_2)) \quad (3c)$$

2) Differentiation properties: Model has different behaviors depending on the engine operating area. Figure 2 details these dependencies on the intake manifold pressure.

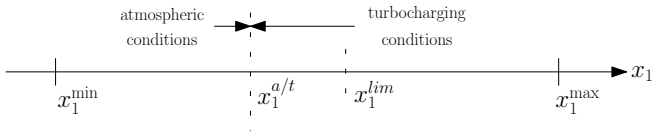

Fig. 2. Engine operating area function of intake manifold pressure x_1.

When the engine is operating under atmospheric conditions, i.e. $x_1 \in [x_1^{\min}; x_1^{a/t}]$, the following model properties hold

$$\frac{\partial f}{\partial x_1} > 0, \ \frac{\partial f}{\partial x_2} > 0, \ \frac{\partial f}{\partial x_3} < 0 \quad (4a)$$
$$\frac{\partial}{\partial x_1}(g^{-1}_{x_1,x_3}) < 0, \ \frac{\partial}{\partial x_1}(g^{-1}_{x_1,x_2}) > 0 \quad (4b)$$
$$\psi' = 0 \quad (4c)$$

Physically, these mean that an increase of the intake manifold pressure x_1 and a decrease of the valve overlap (valve overlap decreases when x_2 increases and x_3 decreases) leads to an increase of the aspirated air mass. The function $g^{-1}_{x_1,x_3}$ represents x_2, while $g^{-1}_{x_1,x_2}$ represents x_3. Inequalities (4b) means that, to keep a constant IGR mass (y_2) while the intake manifold pressure x_1 increases, it is necessary to increase the valve overlap, and then to decrease x_2 and to increase x_3. Finally, property (4c) holds because the intake manifold pressure dynamics does not depend on aspirated air mass. Indeed, the turbocharger feedback loop is at idle.

When the engine is operating under turbocharging conditions, i.e. $x_1 \in [x_1^{a/t}; x_1^{\max}]$, the following model properties hold

$$\frac{\partial f}{\partial x_1} > 0, \begin{cases} \frac{\partial f}{\partial x_2} > 0 \ \forall x_1 \in [x_1^{a/t}; x_1^{lim}[\\ \frac{\partial f}{\partial x_2} < 0 \ \forall x_1 \in]x_1^{lim}; x_1^{\max}] \end{cases}, \ \frac{\partial f}{\partial x_3} > 0 \quad (5a)$$
$$\frac{\partial}{\partial x_1}(g^{-1}_{x_1,x_3}) > 0, \ \frac{\partial}{\partial x_1}(g^{-1}_{x_1,x_2}) < 0 \quad (5b)$$
$$\psi' > 0 \quad (5c)$$

Physically, (5a) means that an increase of the intake manifold pressure increases the aspirated air mass. Variations of f in terms of VVT actuators are a little bit more involved. Actually, differentiating (1) in terms of x_2 and x_3 gives

$$\begin{cases} \frac{\partial f}{\partial x_2} = \frac{\alpha_1 P_{int}}{RT_{int}} \frac{\partial V_{ivc}}{\partial x_2} - \frac{\partial g}{\partial x_2} \\ \frac{\partial f}{\partial x_3} = -\frac{\partial g}{\partial x_3} \end{cases}$$

This means that, when variations of g changes sign, $\frac{\partial f}{\partial x_3}$ changes sign at the same time, but $\frac{\partial f}{\partial x_2}$ does not because of positive term $\frac{\alpha_1 P_{int}}{RT_{int}} \frac{\partial V_{ivc}}{\partial x_2}$. It only switches when the term $\frac{\partial g}{\partial x_2}$ gets high enough, i.e. at x_1^{lim}. Inequalities (5b) means that, to keep a constant IGR mass (y_2), while the intake manifold pressure x_1 increases, it is necessary to decrease the valve overlap, and then to increase x_2 and to decrease x_3. Finally, property (5c) holds because the intake manifold pressure dynamics depends on the aspirated air mass. Indeed, the turbocharger speed increases when the flow going through the turbine increases.

III. Control strategy

We have already shown in [5] that the proposed control strategy is effective under atmospheric conditions. In this paper, we extend it to turbocharging conditions. In addition to the continuity of the control law, we prove that the strategy can improve torque transients results.

The control objective is to track set points for the aspirated air and IGR masses. Consider the global control scheme pictured in Figure 3. A high level-controller feeds three low-level controllers: the intake manifold pressure controller and the two VVT controllers. From $\overline{T_q}$, a torque requested by the driver through the accelerator pedal, and the engine speed N_e, static look-up tables are used to compute aspirated air mass and IGR mass set points, $\overline{y_1}$ and $\overline{y_2}$. Physically, air and IGR masses depend on the intake manifold pressure and the valve gear phasing, i.e. the VVT actuators positions (see model (2)). The high level-controller computes corresponding intake manifold pressure and VVT set points, x_1^{sp}, x_2^{sp} and x_3^{sp}.

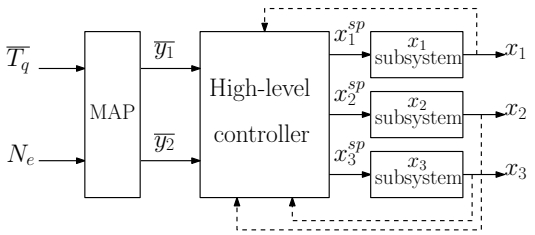

Fig. 3. Control scheme. Dynamic and static controllers fit in the high-level controller block. Only dynamic controller uses feedback loops.

A. Dynamic controller

The control strategy implemented in the high-level controller block in the Figure 3 is presented in [5]. The closed-loops feedback the current values of the intake manifold pressure and the VVT positions. In turn, the high-level controller uses the inverse model derived in Section II-C to

compute set points for the low-level controllers. To account for the slow responses of the corresponding subsystems, these are coordinated by substituting target set points by real-time measurements. Among the numerous possible solutions, we choose a technique which tries to satisfy both aspirated air and IGR masses objectives.

The primary control objective is the aspirated air mass because it directly impacts on the produced torque. By comparison with intake manifold pressure, VVT actuators have limited effect on fresh air charge. Therefore, we use the intake manifold pressure as control variable for air mass control. From an aspirated air mass set point, we compute a pressure set point, x_1^{sp}, using equation (3a). In this formula, *we use VVT actuators positions measurements*.

$$x_1^{sp} = f^{-1}_{x_2,x_3}(\overline{y_1}) \tag{6}$$

From (3a), it is obvious that (6) satisfies the primary control objective.

The secondary control objective is the IGR mass. The two remaining control variables are the VVT actuators. The IGR system is over-actuated. First, we determine the exhaust valve timing, x_3, as $\overline{x_3}$ (defined as a static look-up table function of engine torque and speed). Then, intake valve timing, x_2, remains as possible control variable for the IGR mass control. Its set point x_2^{sp} is computed from IGR mass set point using equation (3b). Again, to coordinate the two control subsystems and maximize speed of transient, *we substitute intake manifold pressure set point with measurements*. Finally, when the control variable x_2^{sp} becomes unfeasible (when intake VVT set point is out of the saturation bounds), it is saturated to the maximum or minimum admissible value, and the left-over degree of freedom, x_3^{sp}, is used to minimize the induced IGR fraction mismatch using equation (3c). The IGR mass control strategy writes

$$\begin{cases} x_2^{sp} = \psi\left(g^{-1}_{x_1,\overline{x_3}}(\overline{y_2})\right) \\ x_3^{sp} = \begin{cases} \overline{x_3} & \text{if } \; x_2^{sp} \in \overset{\circ}{\Omega}_{\Phi_i} \\ \psi\left(g^{-1}_{x_1,x_2^{sp}}(\overline{y_2})\right) & \text{otherwise} \end{cases} \end{cases} \tag{7}$$

where $\overset{\circ}{\Omega}_{\Phi_i}$ is the interior of Ω_{Φ_i} and ψ is the saturation function. From (3b) and (3c), it appears that, provided that at least one of the two VVT positions is not saturated, (7) satisfies the second control objective.

To simplify the theoretical analysis, we summarize the above strategy under the form

$$\text{(dynamic controller)} \begin{cases} x_1^{sp} = f^{-1}_{x_2,x_3}(\overline{y_1}) \\ x_2^{sp} = g^{-1}_{x_1,\overline{x_3}}(\overline{y_2}) \\ x_3^{sp} = g^{-1}_{x_1,\overline{x_2}}(\overline{y_2}) \end{cases} \tag{8}$$

where $\overline{x_2}$ and $\overline{x_3}$ are defined as a static look-up tables function of engine torque and speed.

B. Static controller

To stress the relevance of dynamic controller (8), we compare it to a classical "static" controller. This controller also fits into the global scheme of Figure 3, except that it does not use any feedback loop. The static controller under consideration is

$$\text{(static controller)} \begin{cases} x_1^{sp} = \overline{x_1} = f^{-1}_{\overline{x_2},\overline{x_3}}(\overline{y_1}) \\ x_2^{sp} = \overline{x_2} = g^{-1}_{\overline{x_1},\overline{x_3}}(\overline{y_2}) \\ x_3^{sp} = \overline{x_3} = g^{-1}_{\overline{x_1},\overline{x_2}}(\overline{y_2}) \end{cases} \tag{9}$$

where $\overline{x_1}$, $\overline{x_2}$ and $\overline{x_3}$ are defined as static look-up tables function of engine torque and speed.

IV. Transient analysis

In this section, we compare the controllers (8) and (9) during a large torque tip-in. Figure 4 gives results in terms of aspirated air mass, y_1, intake manifold pressure, x_1, and VVT actuators positions, x_2 and x_3. It is important to notice that, on our experiment, VVT actuators low-level controllers give very poor results (this point will be addressed in future works). We analyze the transient by splitting it into four parts.

A. System definition

Let $\hat{x}_1$, $\hat{x}_2$, $\hat{x}_3$ and $\hat{y}_1$ be the states and output of the system while using the static controller (9). Let $\tilde{x} \triangleq x - \hat{x}$ and $\tilde{y}_1 \triangleq y_1 - \hat{y}_1$. Comparing control strategies (8) and (9) in system (2), yields the following first-order error system

$$\begin{cases} \dot{\tilde{x}}_1 = -(\psi(y_1)x_1 - \psi(\hat{y}_1)\hat{x}_1) + \psi(y_1) f^{-1}_{x_2,x_3}(\overline{y_1}) \\ \qquad\qquad - \psi(\hat{y}_1) f^{-1}_{\overline{x_2},\overline{x_3}}(\overline{y_1}) \\ \dot{\tilde{x}}_2 = -\gamma_2 \tilde{x}_2 + \gamma_2 \left(g^{-1}_{x_1,\overline{x_3}}(\overline{y_2}) - g^{-1}_{\overline{x_1},\overline{x_3}}(\overline{y_2}) \right) \\ \dot{\tilde{x}}_3 = -\gamma_3 \tilde{x}_3 + \gamma_3 \left(g^{-1}_{x_1,\overline{x_2}}(\overline{y_2}) - g^{-1}_{\overline{x_1},\overline{x_2}}(\overline{y_2}) \right) \\ \tilde{y}_1 = \left.\dfrac{\partial f}{\partial x_1}\right|_x \tilde{x}_1 + \left.\dfrac{\partial f}{\partial x_2}\right|_x \tilde{x}_2 + \left.\dfrac{\partial f}{\partial x_3}\right|_x \tilde{x}_3 \end{cases} \tag{10}$$

Further, we consider a first order approximation of function ψ, i.e. $\psi(y_1) = \psi(\hat{y}_1) + \psi'(\hat{y}_1)\tilde{y}_1$. Then, the $\tilde{x}_1$ dynamics reads

$$\begin{aligned} \dot{\tilde{x}}_1 = &-\psi(\hat{y}_1)\tilde{x}_1 - \psi'(\hat{y}_1)x_1\tilde{y}_1 + \psi'(\hat{y}_1) f^{-1}_{x_2,x_3}(\overline{y_1})\tilde{y}_1 \\ &+ \psi(\hat{y}_1)(f^{-1}_{x_2,x_3}(\overline{y_1}) - f^{-1}_{\overline{x_2},\overline{x_3}}(\overline{y_1})) \end{aligned} \tag{11}$$

The terms $f^{-1}_{x_2,x_3}(\overline{y_1})$ and $f^{-1}_{\overline{x_2},\overline{x_3}}(\overline{y_1})$ represent the pressure set points sent to the low-level pressure controller. During such transient, the throttle is wide open and waste gate is fully closed to ensure the maximum speed response of the system. Then, one can neglect the difference between pressure set points. Using (11) in system (10), and defining positive variables γ_1 and β_1 by $\gamma_1 \triangleq \psi(\hat{y}_1) - \beta_1 \left.\frac{\partial f}{\partial x_1}\right|_x$ with $\beta_1 \triangleq \psi'(\hat{y}_1)(f^{-1}_{x_2,x_3}(\overline{y_1}) - x_1)$, the following system is obtained

$$\begin{cases} \dot{\tilde{x}}_1 = -\gamma_1 \tilde{x}_1 + \beta_1 \left.\dfrac{\partial f}{\partial x_2}\right|_x \tilde{x}_2 + \beta_1 \left.\dfrac{\partial f}{\partial x_3}\right|_x \tilde{x}_3 \\ \dot{\tilde{x}}_2 = -\gamma_2 \tilde{x}_2 + \gamma_2 \left(g^{-1}_{x_1,\overline{x_3}}(\overline{y_2}) - g^{-1}_{\overline{x_1},\overline{x_3}}(\overline{y_2}) \right) \\ \dot{\tilde{x}}_3 = -\gamma_3 \tilde{x}_3 + \gamma_3 \left(g^{-1}_{x_1,\overline{x_2}}(\overline{y_2}) - g^{-1}_{\overline{x_1},\overline{x_2}}(\overline{y_2}) \right) \\ \tilde{y}_1 = \left.\dfrac{\partial f}{\partial x_1}\right|_x \tilde{x}_1 + \left.\dfrac{\partial f}{\partial x_2}\right|_x \tilde{x}_2 + \left.\dfrac{\partial f}{\partial x_3}\right|_x \tilde{x}_3 \end{cases} \tag{12}$$

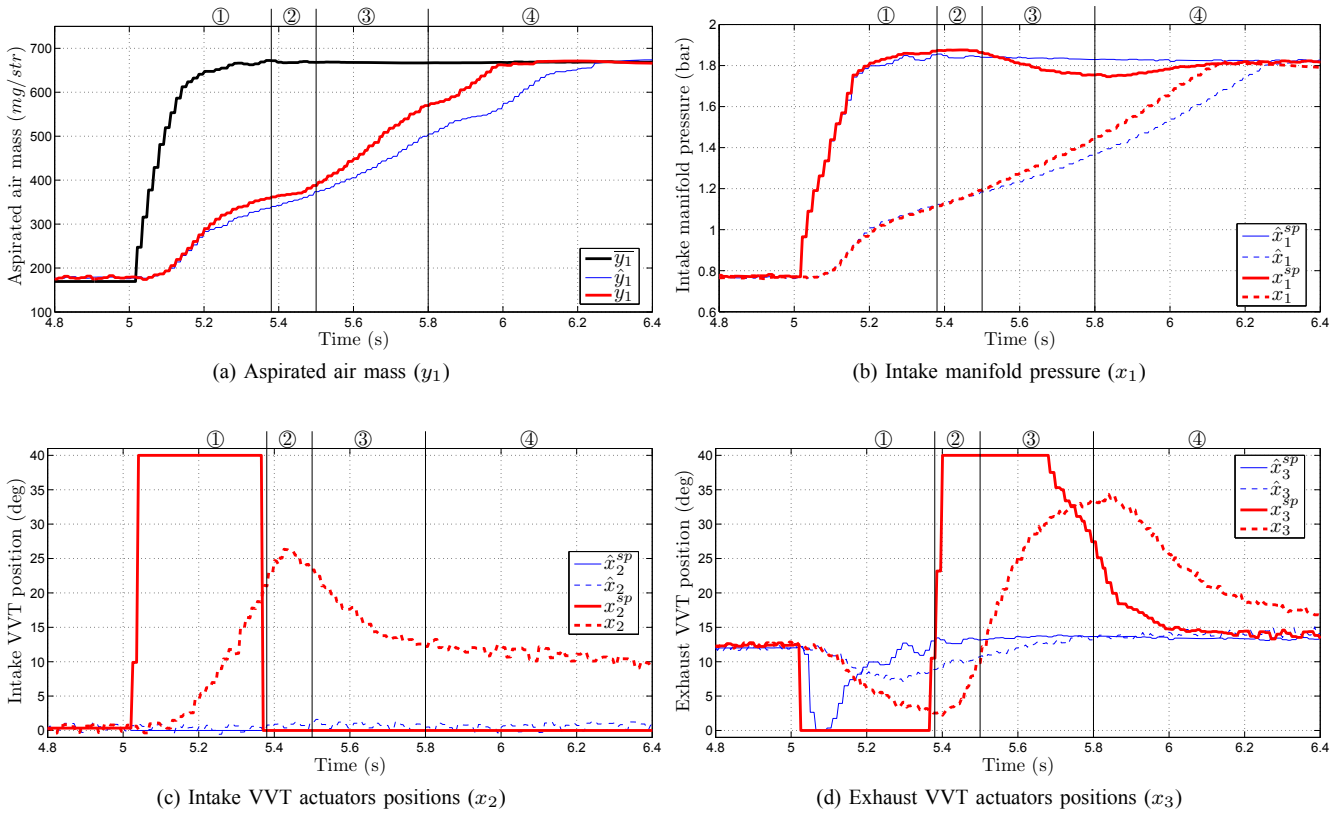

(a) Aspirated air mass (y_1)

(b) Intake manifold pressure (x_1)

(c) Intake VVT actuators positions (x_2)

(d) Exhaust VVT actuators positions (x_3)

Fig. 4. Experimental results on a 4-cylinder turbocharged VVT SI engine at constant engine speed (2000 rpm). Fast torque tip-in corresponding to a transient from atmospheric conditions to turbocharging conditions. Comparison between two control strategies: static controller (9) (corresponding states and output are noted $\hat{x}_1$, $\hat{x}_2$, $\hat{x}_3$ and $\hat{y}_1$) and dynamic controller (8) (corresponding states and output are noted x_1, x_2, x_3 and y_1).

The initial conditions of the error system are $\tilde{x}_1(0) = \tilde{x}_2(0) = \tilde{x}_3(0) = \tilde{y}_1(0) = 0$.

B. *Transient - Part ①*

We start under atmospheric conditions, $x_1 \in [x_1^{\min}; x_1^{a/t}]$. Using the model property (4c) in (12) leads to $\dot{\tilde{x}}_1 = -\psi(\hat{y}_1)\tilde{x}_1$. This stresses that the intake manifold pressure trajectory is not impacted by the VVT actuators positions. Because the initial condition of $\tilde{x}_1$ is zero, then $\tilde{x}_1 = 0$ during part ① of the transient (see Figure 4b).

Let $h_2 : \Omega_p \to \Omega_{\Phi_i}$ and $h_3 : \Omega_p \to \Omega_{\Phi_e}$ be the continuous functions defined by $h_2(x_1) \triangleq g^{-1}_{x_1,\overline{x_3}}(\overline{y_2})$ and $h_3(x_1) \triangleq g^{-1}_{x_1,\overline{x_2}}(\overline{y_2})$. From the intermediate value theorem, there exists c in $[x_1; x_1^{a/t}]$, such that

$$\begin{cases} h_2(x_1) - h_2(x_1^{a/t}) = h_2'(c)(x_1 - x_1^{a/t}) \\ h_3(x_1) - h_3(x_1^{a/t}) = h_3'(c)(x_1 - x_1^{a/t}) \end{cases}$$

From the model properties (4b), and because $x_1 - x_1^{a/t} < 0$, one obtains

$$\begin{cases} g^{-1}_{x_1,\overline{x_3}}(\overline{y_2}) - g^{-1}_{\overline{x_1},\overline{x_3}}(\overline{y_2}) > 0 \\ g^{-1}_{x_1,\overline{x_2}}(\overline{y_2}) - g^{-1}_{\overline{x_1},\overline{x_2}}(\overline{y_2}) < 0 \end{cases} \tag{13}$$

Because the initial conditions of $\tilde{x}_2$ and $\tilde{x}_3$ are both zero, integration of the $\tilde{x}_2$ and $\tilde{x}_3$ dynamics in system (12) using (13) gives $\tilde{x}_2 > 0$ and $\tilde{x}_3 < 0$ during part ① of the transient (see Figure 4c and Figure 4d).

Finally, using model properties (4a) in the output equation of system (12), it comes $\tilde{y}_1 > 0$ during part ① of the transient. It is confirmed by experimental results in Figure 4a.

C. *Transient - Part ②*

In this part of the transient, the engine enters in the turbocharging area, $x_1 \in [x_1^{a/t}; x_1^{lim}]$.

Again, from the intermediate value theorem, there exists one real c in $[x_1; x_1^{lim}]$, such that

$$\begin{cases} h_2(x_1) - h_2(x_1^{lim}) = h_2'(c)(x_1 - x_1^{lim}) \\ h_3(x_1) - h_3(x_1^{lim}) = h_3'(c)(x_1 - x_1^{lim}) \end{cases}$$

From model properties (5b) and as $x_1 - x_1^{lim} < 0$, it comes

$$\begin{cases} g^{-1}_{x_1,\overline{x_3}}(\overline{y_2}) - g^{-1}_{\overline{x_1},\overline{x_3}}(\overline{y_2}) < 0 \\ g^{-1}_{x_1,\overline{x_2}}(\overline{y_2}) - g^{-1}_{\overline{x_1},\overline{x_2}}(\overline{y_2}) > 0 \end{cases} \tag{14}$$

The input terms driving the $\tilde{x}_2$ and $\tilde{x}_3$ both change sign. Due to the positive and negative initial conditions obtained at the end of the part ①, $\tilde{x}_2$ and $\tilde{x}_3$ remains positive and negative respectively until the end of part ②. Interestingly, on the experiment, an additional lag helps $\tilde{x}_2$ to increase at the beginning of this part (which is not represented by the first order approximation of system (2)). Looking at output model

properties (5a), it appears that the products $\frac{\partial f}{\partial x_2}\tilde{x}_2$ and $\frac{\partial f}{\partial x_3}\tilde{x}_3$ are positive and negative, respectively. Experimentally, we have

$$\frac{\partial f}{\partial x_2}\tilde{x}_2 + \frac{\partial f}{\partial x_3}\tilde{x}_3 > 0 \tag{15}$$

On the observed transient, condition (15) depend on the performance of the VVT actuators. In theory, these should track accurately their set points. This would imply $\tilde{x}_2 \simeq 0$ and $\tilde{x}_3 > 0$. The mentioned assumption (15) would then be automatically satisfied. On the other hand, it shall be noted that a worst-case scenario exists, when the exhaust VVT are very slow and the intake VVT are very fast. Under these conditions, the assumption (15) fails, and may damage the overall performance.

Considering (15), and because the initial condition of $\tilde{x}_1$ (from part ② of the transient) is zero, integration of the $\tilde{x}_1$ dynamics in system (12) gives $\tilde{x}_1 > 0$ during part ② of the transient.

Finally, using model properties (5a) in the output equation of system (12), it comes $\tilde{y}_1 > 0$ during part ② of the transient. It is confirmed by experimental results in Figure 4a.

D. Transient - Part ③

In this part of the transient, $\tilde{x}_3$ is positive. Then, $\frac{\partial f}{\partial x_3}\tilde{x}_3$ is now positive. Consequently, (15) holds and then $\tilde{x}_1 > 0$ and $\tilde{y}_1 > 0$ during part ③ of the transient, see Figure 4b and Figure 4a.

E. Transient - Part ④

In this part of the transient, $x_1 \in [x_1^{lim}; x_1^{\max}]$. From the property (5a), $\frac{\partial f}{\partial x_2}\tilde{x}_2$ is negative, it means that the intake VVT actuator does not increase the aspirated air mass any more. However, experimentally, (15) holds in this part of the transient (if the VVT actuators are accurately controlled and track their set points, (15) is of course satisfied). The $\tilde{x}_1$ dynamics in system (12) gives $\tilde{x}_1 > 0$ during part ④ of the transient.

Finally, using model properties (5a) in the output equation of system (12), yields $\tilde{y}_1 > 0$ during part ④ of the transient. It is confirmed by the experimental results reported in Figure 4a.

F. Torque response

We have shown that the aspirated air mass can be rendered faster during a large torque transient using the proposed dynamic controller (8). Figure 5 confirms that the same good behavior is observed on the engine torque output. Measured torque is given thanks to in-cylinder pressure sensors. Despite a problem at the beginning of the transient (due to poor injection pressure control), we obtain more than 20% gain in terms of time response. The use of a dynamic control strategy to pilot the VVT actuators permits to decrease the acceleration time on turbocharged SI engines.

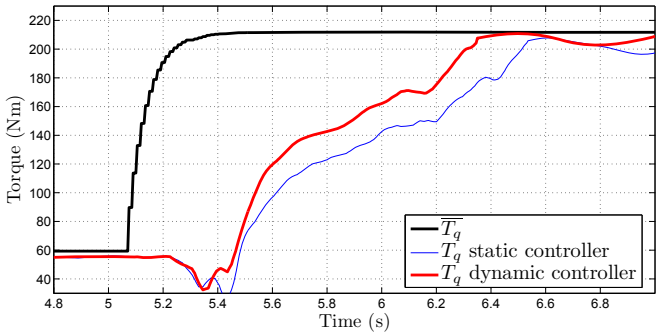

Fig. 5. Torque trajectory during a large torque tip-in corresponding to a transient from atmospheric conditions to turbocharging conditions. Comparison between two control strategies: static controller (9) and dynamic controller (8).

CONCLUSION AND FUTURE DIRECTION

The paper presents an extension of a previous work proposing a control strategy to manage both the aspirated air mass and the internal recirculation gas mass on turbocharged SI engines equipped with VVT actuators. The extension concerns the turbocharging experimental conditions. We show that the same control strategy permits to improve torque transient response time in this extended range. Experimental results obtained at test-bench stress the relevance of the control strategy. At the light of the obtained results, it appears that much improvement can be expected by forcing the low-level VVT controllers to track their set points with more accuracy. Yet, the proposed strategy appears to be quite robust.

We plan to implement the control strategy on a vehicle.

REFERENCES

[1] J. Heywood, *Internal Combustion Engine Fundamentals*. McGraw-Hill, Inc, 1988.

[2] B. Lecointe and G. Monnier, "Downsizing a Gasoline Engine Using Turbocharging with Direct Injection," in *Proc. of SAE Conference*, no. 2003-01-0542, 2003.

[3] T. Leroy, J. Chauvin, F. Le Berr, A. Duparchy, and G. Alix, "Modeling Fresh Air Charge and Residual Gas Fraction on a Dual Independant Variable Valve Timing SI Engine," in *SAE Int. J. Engines*, vol. 1, 2008, pp. 627–635.

[4] A. Stefanopoulou and I. Kolmanovsky, "Analysis and control of transient torque response in engines with internal exhaust gas recirculation," *Control Systems Technology, IEEE Transactions on*, vol. 7, no. 5, pp. 555–566, 1999.

[5] T. Leroy, J. Chauvin, and N. Petit, "Controlling Air and Burned Gas Masses of Turbocharged VVT SI Engines," in *Proc. of the 47th IEEE Conference on Decision and Control*, 2008.

[6] M. Jankovic, "Nonlinear Control in Automotive Engine Applications," in *in Proc. of 15th International Symposium on Mathematical Theory of Networks and Systems*, 2002.

[7] A. Stefanopoulou, I. Kolmanovsky, and J. Freudenberg, "Control of Variable Geometry Turbocharged Diesel Engines for reduced emissions," in *IEEE Transactions on Control Systems Technology*, vol. 8, no. 4, 2000, pp. 733 – 745.

[8] D. Schwarzmann, R. Nitsche, and J. Lunze, "Diesel boost pressure control using flatness-based internal model control," in *Proc. of SAE Conference*, no. 2006-01-0855, 2006.

[9] A. Genç, K. Glover, and R. Ford, "Nonlinear control of hydraulic actuators in variable cam timing engines," in *International IFAC Workshop on Modeling, Emissions and Control in Automotive Engines*, 2001.

[10] L. Guzzella and C. Onder, *Introduction to Modeling and Control of Internal Combustion Engine Systems*. Springer, 2004.